

Cosmological Prediction of the Void and Galaxy Clustering Measurements in the CSST Spectroscopic Survey

YINGXIAO SONG,^{1,2} QI XIONG,^{1,2} YAN GONG*,^{1,2,3} FUREN DENG,^{1,2} KWAN CHUEN CHAN,^{4,5} XUELEI CHEN,^{1,2,6,7}
QI GUO,^{1,2} GUOLIANG LI,⁸ MING LI,¹ YUN LIU,^{1,2} YU LUO,^{9,8} WENXIANG PEI,^{1,2} AND CHENGLIANG WEI⁸

¹*National Astronomical Observatories, Chinese Academy of Sciences, 20A Datun Road, Beijing 100012, China*

²*School of Astronomy and Space Sciences, University of Chinese Academy of Sciences(UCAS),
Yuquan Road NO.19A Beijing 100049, China*

³*Science Center for China Space Station Telescope, National Astronomical Observatories, Chinese Academy of Sciences,
20A Datun Road, Beijing 100101, China*

⁴*School of Physics and Astronomy, Sun Yat-sen University, 2 Daxue Road, Tangjia, Zhuhai, 519082, China*

⁵*CSST Science Center for the Guangdong-Hongkong-Macau Greater Bay Area, SYSU, Zhuhai, 519082, China*

⁶*Department of Physics, College of Sciences, Northeastern University, Shenyang 110819, China*

⁷*Centre for High Energy Physics, Peking University, Beijing 100871, China*

⁸*Purple Mountain Observatory, Chinese Academy of Sciences, Nanjing, 210023, PR China*

⁹*Department of Physics, School of Physics and Electronics, Hunan Normal University, Changsha 410081, PR China*

ABSTRACT

The void power spectrum is related to the clustering of low-density regions in the large-scale structure (LSS) of the Universe, and can be used as an effective cosmological probe to extract the information of the LSS. We generate the galaxy mock catalogs from Jiutian simulation, and identify voids using the watershed algorithm for studying the cosmological constraint strength of the China Space Station Telescope (CSST) spectroscopic survey. The galaxy and void auto power spectra and void-galaxy cross power spectra at $z = 0.3, 0.6,$ and 0.9 are derived from the mock catalogs. To fit the full power spectra, we propose to use the void average effective radius at a given redshift to simplify the theoretical model, and adopt the Markov Chain Monte Carlo (MCMC) technique to implement the constraints on the cosmological and void parameters. The systematical parameters, such as galaxy and void biases, and noise terms in the power spectra are also included in the fitting process. We find that our theoretical model can correctly extract the cosmological information from the galaxy and void power spectra, which demonstrates its feasibility and effectivity. The joint constraint accuracy of the cosmological parameters can be improved by $\sim 20\%$ compared to that from the galaxy power spectrum only. The fitting results of the void density profile and systematical parameters are also well constrained and consistent with the expectation. This indicates that the void clustering measurement can be an effective complement to the galaxy clustering probe, especially for the next generation galaxy surveys.

Keywords: Cosmology(343), Voids (1779), Cosmological parameters (339), Large-scale structure of the universe (902)

1. INTRODUCTION

On the cosmic scale, the observable universe has a distribution of matter with a network-like structure (Bond et al. 1996), and there are obvious filamentary struc-

tures connecting them between the galaxy clusters. In the space between these superstructures, galaxy spectroscopic surveys find some regions with large volume and low galaxy density, which are called cosmic voids (Gregory & Thompson 1978; Jõeveer et al. 1978; Kirshner et al. 1981; de Lapparent et al. 1986). Nowadays, as extensive galaxy surveys provide sufficient galaxy samples in vast space volumes, cosmic void has become an effective cosmological probe in the studies of cosmic large-

scale structure (LSS), such as the void abundance (e.g. Contarini et al. 2021, 2022, 2023; Pellicciari et al. 2023; Song et al. 2024; Verza et al. 2024), Alcock-Paczyński effect (AP), redshift space distortions (RSD) (e.g. Nadathur & Percival 2019; Nadathur et al. 2020; Correa et al. 2021, 2022; Hamaus et al. 2022), and baryonic acoustic oscillations (BAO) (e.g. Chan & Hamaus 2021; Forero-Sánchez et al. 2022; Khoraminezhad et al. 2022). Cosmic voids are also used in studying modified gravity and massive neutrinos (e.g. Cai et al. 2015; Pisani et al. 2015; Zivick et al. 2015; Pollina et al. 2016; Achitouv 2016; Sahlén et al. 2016; Falck et al. 2018; Sahlén & Silk 2018; Paillas et al. 2019; Perico et al. 2019; Verza et al. 2019; Kreisch et al. 2019; Schuster et al. 2019; Contarini et al. 2021; Kreisch et al. 2022; Mauland et al. 2023; Verza et al. 2023; Vielzeuf et al. 2023).

Galaxy spectroscopic surveys can map the LSS by providing information on the positions of galaxies in three dimensions, such as Baryon Oscillation Spectroscopic Survey (BOSS, Alam et al. 2017) and Dark Energy Spectroscopic Instrument (DESI, DESI Collaboration et al. 2016). The analysis of such data usually focuses on the auto correlation of galaxies, especially the two-point galaxy correlation function (2PCF) and power spectrum. However, galaxy statistics may only provide a part of the LSS information, and we can expect that the LSS probably can be better studied by taking voids into account.

The void-galaxy cross-correlation has been studied in a number of relevant works (e.g. Cai et al. 2016; Nadathur & Percival 2019; Woodfinden et al. 2022; Hamaus et al. 2022; Radinović et al. 2023; Mauland et al. 2023), which is proven to be an effective cosmological probe for extracting the information of the LSS. In this work, we discuss the auto and cross correlations of void and galaxy in the China Space Station Telescope (CSST, Zhan 2011, 2021; Gong et al. 2019; Miao et al. 2023) spectroscopic survey, and propose to use the mean void radius at a given redshift to simplify the theoretical calculation based on the halo model for fitting the full power spectra.

To check the feasibility of this method, we generate the mock galaxy catalogs from Jiutian simulations, and take into account the CSST survey strategy and instrumental design. Then we identify voids in the galaxy catalogs using Voronoi tessellation and watershed algorithm. The void and galaxy auto and cross power spectra at $z = 0.3, 0.6, 0.9$ are derived from the void and galaxy mock catalogs. After the theoretical modeling of the power spectra, we perform the constraints on the cosmological and void parameters in our model using the Markov Chain Monte Carlo (MCMC) method. The galaxy and

void biases and noise terms are also considered in the analysis.

The paper is organized as follows: in Section 2, we introduce the creation of galaxy and void mock catalogs of the CSST spectroscopic surveys. In Section 3, we estimate the galaxy, void and the void-galaxy power spectra from the mock catalogs and calculate the corresponding theoretical models. In Section 4, we discuss the constraint results of the model parameters. We summarize our work in Section 5.

2. MOCK CATALOGS

2.1. Simulation

We adopt the high-resolution dark-matter-only Jiutian N-body simulations to serve as the basis for generating galaxy catalog. The Jiutian simulation we use covers a volume of $1 (h^{-1}\text{Gpc})^3$ and contains 6144^3 particles with a mass resolution of $m_p = 3.72 \times 10^8 h^{-1} M_\odot$. There are totally 128 snapshot outputs from initial redshift $z_i = 127$ down to redshift $z = 0$. The simulation is performed by running the L-Gadget3 code, and uses friend-of-friend and subfind algorithm to identify the dark matter halo and substructure (Springel et al. 2001; Springel 2005). The best-fit values of the cosmological parameters from *Planck*2018 are set as fiducial values in the simulation, i.e. $h = 0.6766$, $\Omega_m = 0.3111$, $\Omega_b = 0.0490$, $\Omega_\Lambda = 0.6899$, $\sigma_8 = 0.8102$ and $n_s = 0.9665$ (Planck Collaboration et al. 2020).

Considering the RSD and structure evolution effects, we construct each simulation cube with a few slices based on the snapshot outputs at different redshifts. We choose the line-of-sight (LOS) parallel to the edge of the box, and then splice slice-like halo catalogs together according to their comoving distances. In our mock catalog, we address the evolution effects by tracing the merger tree of each galaxy to find the snapshot with the closest redshift corresponding to the distance of galaxy. Our method naturally avoids repetition or omission of galaxies at the boundary of slices, compared to directly slicing and stitching the snapshots by redshift. For a reliable RSD calculation, we do not perform the interpolation when splicing the slices, and it will not affect our result at the scales and accuracies we are interested in. We construct three simulation cubes with the central redshift $z_c = [0.3, 0.6, 0.9]$ to build our galaxy and void mock catalogs.

2.2. Galaxy mock catalog

We study the CSST spectroscopic survey for exploring the void and galaxy clustering measurements. The CSST contains slitless grating spectrograph with three bands i.e. *GU*, *GV* and *GI*, and covers wavelength

range 225-1000 nm. It will launch in 2026 and plan to survey 17500 deg² sky area in about ten years. The angular resolution is $\sim 0.3''$ with 80% energy concentration for the spectroscopic survey, and the spectral resolution $R = \lambda/\Delta\lambda$ is better than 200. The magnitude limit can reach ~ 23 AB mag for 5σ point source detection in a band.

We construct the mock galaxy catalog using an updated version of the L-Galaxies semi-analytical model (Springel 2005; Croton et al. 2006; De Lucia & Blaizot 2007; Guo et al. 2011), which includes improvements for handling the disruption of satellite galaxies and the growth of supermassive black holes compared to the version from Henriques et al. (2015). This new model also includes additional features related to galaxy properties, such as the incorporation of galaxy emission line luminosity produced through post-processing techniques (Pei et al. 2024). We can use these emission lines to derive precise spectroscopic redshift and select galaxies that can be detected by the CSST spectroscopic survey. For each galaxy, the redshift z involves the peculiar motions of the source z_{pec} and cosmological redshift z_{cos} , and the relation is $1 + z = (1 + z_{\text{cos}})(1 + z_{\text{pec}}) = (1 + z_{\text{cos}})(1 + v_{\text{pec}}/c)$, where v_{pec} is the LOS component of peculiar velocity. Besides, we also assign a redshift uncertainty $\sigma = 0.002$ to each galaxy for counting the accuracy of the CSST slitless spectral calibration.

We select galaxies by the signal-to-noise ratio (SNR), and consider four emission lines to estimate the SNR, i.e. H α , H β , [OIII] and [OII]. Since the region of an emission line is usually small compare to the full size of a galaxy, we simply treat galaxies as point sources in the estimation. For a space telescope, the SNR per spectral resolution unit for a spectroscopic sample can be calculated by (Cao et al. 2018; Deng et al. 2022)

$$\text{SNR} = \frac{C_s t_{\text{exp}} \sqrt{N_{\text{exp}}}}{\sqrt{C_s t_{\text{exp}} + N_{\text{pix}}[(B_{\text{sky}} + B_{\text{det}})t_{\text{exp}} + R_n^2]}}, \quad (1)$$

where $N_{\text{pix}} = \Delta A/l_p^2$ is the number of detector pixels covered by an object. Here ΔA is the pixel area on the detector, assumed to be the same for all galaxies for simplicity. $l_p = 0.074''$ is the pixel size, and the point-spread function (PSF) is assumed based on the angular resolution of the CSST spectroscopic survey. $N_{\text{exp}} = 4$ is the number of exposures and $t_{\text{exp}} = 150$ s is the exposure time. $R_n = 5 e^{-\text{s}^{-1}\text{pixel}^{-1}}$ is the read noise, and $B_{\text{det}} = 0.02 e^{-\text{s}^{-1}\text{pixel}^{-1}}$ is the dark current of the detector. B_{sky} is the sky background in $e^{-\text{s}^{-1}\text{pixel}^{-1}}$, and C_s is the counting rate from a galaxy. We find that $B_{\text{sky}} = 0.016, 0.196,$ and $0.266 e^{-\text{s}^{-1}\text{pixel}^{-1}}$ for *GU*, *GV* and *GI* bands, respectively (Song et al. 2024).

We select galaxies if $\text{SNR} \geq 10$ for any emission line of the four lines mentioned above in any spectroscopic band to get the galaxy mock catalog. We find that the number density of galaxies are $\bar{n} = 1.5 \times 10^{-2}, 2.1 \times 10^{-3}, 4.6 \times 10^{-4} h^3 \text{Mpc}^{-3}$ for the three redshift bins we choose at $z = 0.3, 0.6, 0.9$, respectively. This is basically consistent with the previous studies (e.g. Gong et al. 2019).

2.3. Void mock catalog

We identify voids in our mock galaxy catalog using Void IDentification and Examination toolkit¹ (VIDE, Sutter et al. 2015), which is based on ZONes Bordering On Voidness (ZOBOV, Neyrinck 2008). This code identifies voids by Voronoi tessellation and using the watershed algorithm (Platen et al. 2007), which finds voids with more natural shapes without any shape assumption. It also can provide useful void information, such as void effective radius and volume-weighted center. Note that we use the low-density zones that are not merged before to avoid void-in-void case when generating the void catalog.

The voids identified by VIDE are composed of cells containing a galaxy inside, and the total volume V of each void is the sum of all the cell volumes it contains. Based on the volume and position of each cell we can get the void effective radius R_v from V , and the volume-weighted center of the void \mathbf{X}_v can be estimated by

$$\mathbf{X}_v = \frac{1}{V} \sum_i^N \mathbf{x}_i V_{\text{cell}}^i. \quad (2)$$

Here $V = \sum V_{\text{cell}}^i = 4/3\pi R_v^3$, V_{cell}^i is the volume of a cell, and \mathbf{x}_i is the coordinate of the galaxy within a cell in a given void.

In Table 1, we show the number densities of galaxy and void in different redshift bins from the mock catalogs. We filter out voids with the effective radius $R_v < 5 h^{-1}\text{Mpc}$ to avoid the effects of nonlinear evolution. We also show the average, minimum and maximum radius of voids with $R_v > 5 h^{-1}\text{Mpc}$. We can find that the number density of voids have the similar trend of the galaxy number density, which decreases from $z = 0.3$ to 0.9 , and the mean void radius becomes larger and larger as redshift increases.

3. POWER SPECTRUM

The galaxy power spectrum in redshift space $P_{\text{AB}}^s(k, \mu)$ for two kinds of tracers A and B can be esti-

¹ https://bitbucket.org/cosmicvoids/vide_public/src/master/

Table 1. The number densities of galaxy and void (with $R_v > 5 h^{-1}\text{Mpc}$), i.e. n_g and n_v (in $h^3\text{Mpc}^{-3}$), in our mock catalogs at $z = 0.3, 0.6, 0.9$. The mean, minimum and maximum radius of voids (in $h^{-1}\text{Mpc}$) are also shown.

z	n_g	n_v	R_v^{mean}	R_v^{min}	R_v^{max}
0.3	1.5×10^{-2}	4.8×10^{-5}	11.0	5	45
0.6	2.1×10^{-3}	1.0×10^{-5}	19.7	5	70
0.9	4.6×10^{-4}	2.9×10^{-6}	31.4	6	90

mated using the power spectrum in real space $P_{\text{AB}}(k)$, and we have

$$P_{\text{AB}}^s(k, \mu) = P_{\text{AB}}(k)(1 + \beta\mu^2)^2 \mathcal{D}(k, \mu), \quad (3)$$

where the superscript ‘‘s’’ denotes the redshift space, k is the wavenumber, $\mu = k_{\parallel}/k$ is the cosine of the angle between line of sight and k . $\beta = f/b_g$, where b_g is the galaxy linear bias and f is the growth rate. $\mathcal{D}(k, \mu) = \exp[-(k\mu\sigma_{\text{D}})^2]$ is the damping term at small scales. Here $\sigma_{\text{D}}^2 = \sigma_{\text{R}}^2 + \sigma_v^2$, where $\sigma_{\text{R}} = c\sigma_z/H(z)$ is the smearing factor when the power spectrum at the scales smaller than the spectral resolution in the spectroscopic surveys. And $\sigma_z = (1+z)\sigma_z^0$ (Wang et al. 2009), we assume $\sigma_z^0 = 0.002$ considering the accuracy of the CSST slitless spectral calibration. For the velocity dispersion $\sigma_v = \sigma_{v0}(1+z)$ (Scoccimarro 2004; Taruya et al. 2010), we set $\sigma_{v0} = 7 \text{ Mpc}/h$ for the CSST measured emission-line galaxies (Gong et al. 2019). Note that this damping term does not affect our result significantly, since we mainly focus on the linear regime at large scales.

For galaxies as tracers, the real-space galaxy auto power spectrum at z can be estimated by

$$P_{\text{gg}}(k, z) \simeq b_g^2 P_{\text{mm}}(k, z) + N_g(z), \quad (4)$$

where N_g is the galaxy noise term, including the shot noise and systematics in the CSST slitless spectral calibration (Gong et al. 2019). $P_{\text{mm}}(k, z)$ is the matter power spectrum at z , and we calculate it using CAMB in this work (Lewis et al. 2000).

When voids act as tracers, the void auto power spectrum can be estimated by integrating over the void radius based on the halo model as given by Hamaus et al. (2014b). In a narrow range of R_v , the void power spectrum in real space at z can be simplified as

$$P_{\text{vv}}(k, z) \simeq [b_v(z) u_v(k, z)]^2 P_{\text{mm}}(k, z) + N_v(z). \quad (5)$$

Here $b_v(z)$ is the void bias, and N_v is the noise term dominated by the shot noise for voids. $u_v(k)$ is the void

density profile in Fourier space, and it can be obtained from the configuration space by

$$u_v(k) = \frac{\bar{\rho}}{\delta m} \int_{R_v^{\text{min}}}^{R_v^{\text{max}}} u_v(r) \frac{\sin(kr)}{kr} 4\pi r^2 dr, \quad (6)$$

where δm is the void uncompensated mass as a normalization factor, which is calculated by

$$\delta m = \bar{\rho} \int_{R_v^{\text{min}}}^{R_v^{\text{max}}} u_v(r) 4\pi r^2 dr. \quad (7)$$

Here $u_v(r)$ is the void density profile, which denotes spherically averaged deviation of the void mass density from the mean matter density of the entire universe. It can be calculated using an empirical formula called HSW profile, and it is given by (Hamaus et al. 2014a)

$$u_v(r) = \frac{\rho_v(r)}{\bar{\rho}} - 1 = \delta_{\text{cen}} \frac{1 - (r/R_s)^\alpha}{1 + (r/R_v)^\beta}, \quad (8)$$

where ρ_v is the void density, $R_s \equiv \gamma R_v$ is the scale radius when $\rho_v = \bar{\rho}$, δ_{cen} is the central density contrast, and it can be cancelled out in the calculation as shown in Equation (6). α , β and γ denote the inner, outer slope of compensation wall around the void, and ratio of scale radius relative to void radius, respectively, and we set them as free parameters which can be jointly fitted in the model fitting process.

Here we propose to use the mean void effective radius R_v^{mean} to simplify the calculation, by setting $R_v = R_v^{\text{mean}}$ in Equation (8). This means R_s , $u_v(r)$ and $u_v(k)$, as well as α , β and γ , can be seen as the mean values of all selected voids at z . Then we can use Equation (5) to calculate the void auto power spectrum as a good approximation.

Similarly, we can estimate the void-galaxy cross power spectrum at z by (Hamaus et al. 2014b)

$$P_{\text{vg}}(k) = b_v b_g u_v(k) P_{\text{mm}}(k) + N_v u_v(k) + N_{\text{vg}}, \quad (9)$$

where N_{vg} is the noise term for the cross correlation. Besides the three parameters in the HSW profile, we also set the galaxy bias b_g , void bias b_v , and noise terms of the auto and cross power spectra at a given redshift as free parameters, which can provide proper flexibility to explore the distribution of voids in the LSS at different redshifts.

Integrating $P_{\text{AB}}^s(k, \mu)$ over μ and considering the Alcock-Paczyński effect (AP, Alcock & Paczynski 1979), we can obtain the multipole power spectrum, which is given by

$$P_\ell^{\text{AB}}(k) = \frac{2\ell + 1}{2\alpha_\perp^2 \alpha_\parallel} \int_{-1}^1 P_{\text{AB}}^s(k', \mu') \mathcal{L}_\ell(\mu) d\mu. \quad (10)$$

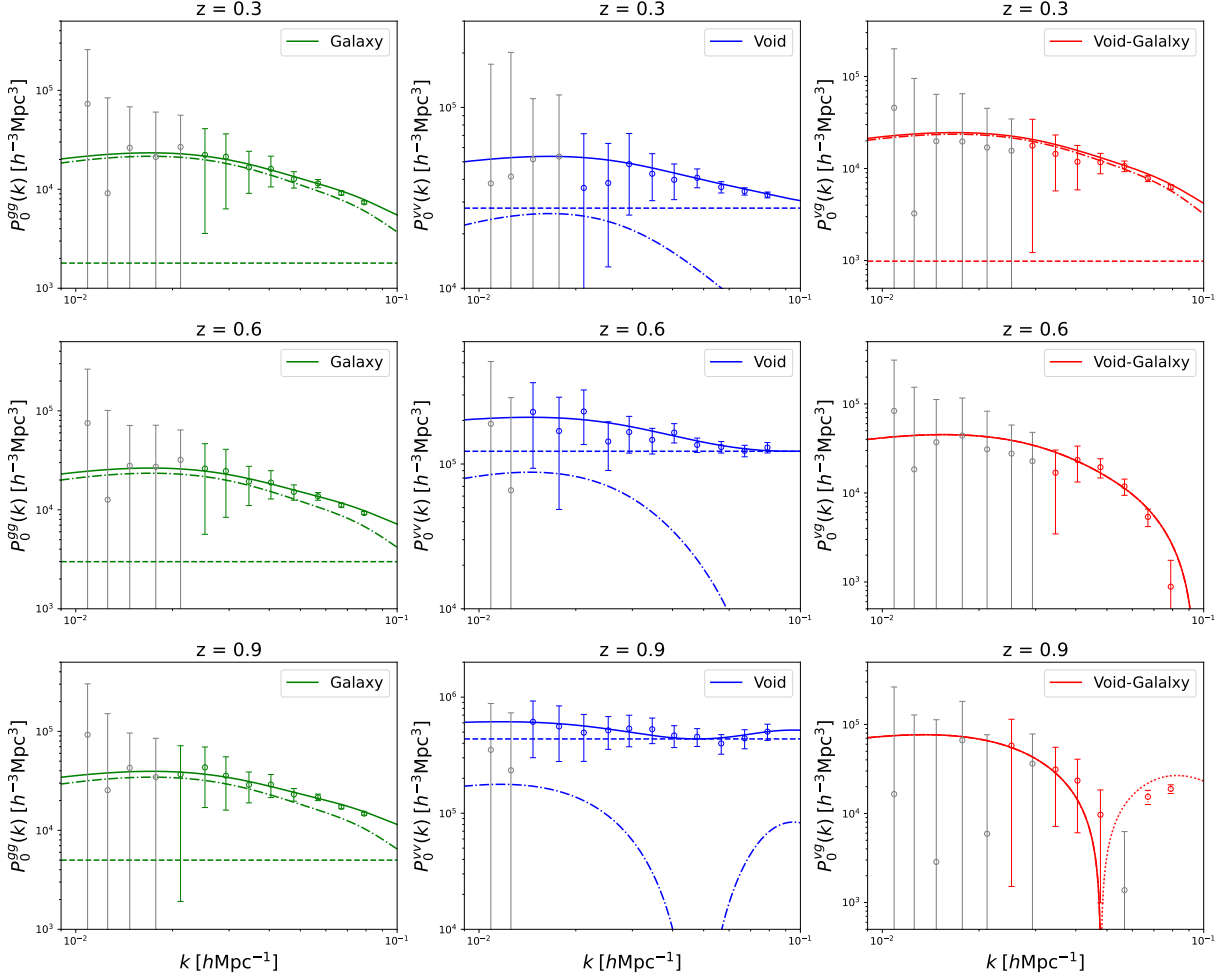


Figure 1. The multipole power spectra P_ℓ^{gg} (green), P_ℓ^{vv} (blue) and P_ℓ^{vg} (red) with $\ell = 0$ at $z = 0.3, 0.6$ and 0.9 in the simulation. The gray data points with $\text{SNR} < 1$ are excluded in the constraint process. The curves are the best-fits of the theoretical calculation, and the dotted line indicates that the values are negative. The solid, dash-dotted and dashed curves are the total, clustering and noise terms of the power spectra.

Here $\mathcal{L}_\ell(\mu)$ is the Legendre polynomials, and only the non-vanishing components $\ell = (0, 2, 4)$ need to be considered. $\alpha_\perp = D_A(z)/D_A^*(z)$ is the transverse scaling factor and $\alpha_\parallel = H^*(z)/H(z)$ is the radial scaling factor. The superscript “*” means the fiducial cosmology. Note that, we only consider the multipole power spectra with $\ell = 0$ as an example in this work, since the data for $\ell = 2$ and 4 have large errors and low SNRs limited by the simulation size. We can use the full multipole power spectra with $\ell = (0, 2, 4)$ in the real CSST or other Stage IV surveys with large sky coverage.

For generating the mock data of the void and galaxy power spectra, we make use of `powerbox` (Murray 2018) to derive the data points, and the errors are estimated by using the jackknife method. In order to obtain sufficient statistical significance in the fitting process, we only use the data points with $\text{SNR} > 1$. In Figure 1, we show the mock data of the galaxy, void and void-galaxy

multipole power spectra with $\ell = 0$ at $z = 0.3, 0.6$ and 0.9 . We note that, due to the limitation of the size of simulation box, the data points have quite large errors and variances at large scales with $k \lesssim 0.02 h/\text{Mpc}$. This issue can be significantly improved in the real CSST or other Stage IV surveys, covering several thousands or more than ten thousand square degrees.

4. CONSTRAINT AND RESULTS

The χ^2 method is adopted to fit the mock data of void, galaxy and void-galaxy power spectra, which takes the form as

$$\chi_{\text{AB}}^2 = \sum \frac{[P_{\text{data}}^{\text{AB}}(k, z) - P_{\text{th}}^{\text{AB}}(k, z)]^2}{\sigma_{\text{data}}^2}, \quad (11)$$

Table 2. The fiducial values, flat prior, best-fit values and errors of the six cosmological parameters, three void density profile parameters $\alpha^i, \beta^i, \gamma^i$, and the void biases b_v^i at $z = 0.3, 0.6$, and 0.9 . The relative constraint accuracies of the parameters are also shown. Note that these results are derived from the simulations limited by the box size. If considering the $17,500 \text{ deg}^2$ full sky coverage of the CSST, the constraint accuracy can be improved by about one order of magnitude.

Parameter	Fiducial value	Flat prior	Constraints by galaxy clustering	Constraints by void clustering	Joint constraints
Cosmology					
w	-1	(-1.8, -0.2)	$-1.117_{-0.472}^{+0.507}$ (43.8%)	$-0.824_{-0.710}^{+0.522}$ (74.7%)	$-1.207_{-0.431}^{+0.444}$ (36.2%)
h	0.6766	(0.5, 0.9)	$0.609_{-0.067}^{+0.094}$ (13.2%)	$0.603_{-0.076}^{+0.166}$ (20.0%)	$0.600_{-0.059}^{+0.066}$ (10.4%)
Ω_m	0.3111	(0.1, 0.5)	$0.362_{-0.090}^{+0.089}$ (24.6%)	$0.313_{-0.151}^{+0.133}$ (45.3%)	$0.371_{-0.082}^{+0.082}$ (22.1%)
Ω_b	0.049	(0.02, 0.08)	$0.042_{-0.016}^{+0.021}$ (44.5%)	$0.047_{-0.019}^{+0.022}$ (43.2%)	$0.035_{-0.011}^{+0.021}$ (45.5%)
n_s	0.9665	(0.7, 1.2)	$0.884_{-0.126}^{+0.156}$ (15.9%)	$1.022_{-0.217}^{+0.132}$ (17.1%)	$0.921_{-0.144}^{+0.168}$ (17.0%)
$A_s (\times 10^{-9})$	2.1	(1.0, 3.0)	$2.049_{-0.647}^{+0.622}$ (30.9%)	$1.827_{-0.623}^{+0.770}$ (38.1%)	$1.920_{-0.526}^{+0.654}$ (30.7%)
Void					
α^1	-	(0, 10.0)	-	$2.978_{-2.135}^{+3.775}$ (99.2%)	$2.216_{-1.579}^{+2.587}$ (94%)
α^2	-	(0, 10.0)	-	$2.915_{-1.935}^{+3.660}$ (96.0%)	$4.448_{-3.074}^{+3.265}$ (71.3%)
α^3	-	(0, 10.0)	-	$3.149_{-2.333}^{+3.973}$ (100.1%)	$1.878_{-1.351}^{+2.366}$ (99.0%)
β^1	-	(0, 20.0)	-	$9.501_{-5.832}^{+5.649}$ (60.4%)	$11.275_{-3.784}^{+4.867}$ (38.4%)
β^2	-	(0, 20.0)	-	$10.700_{-4.149}^{+5.519}$ (45.2%)	$11.893_{-2.890}^{+3.510}$ (26.9%)
β^3	-	(0, 20.0)	-	$14.657_{-4.823}^{+3.239}$ (27.5%)	$14.122_{-2.825}^{+2.077}$ (17.4%)
γ^1	-	(0, 2.0)	-	$0.706_{-0.516}^{+0.824}$ (94.9%)	$0.438_{-0.301}^{+0.418}$ (82.0%)
γ^2	-	(0, 2.0)	-	$0.709_{-0.506}^{+0.792}$ (91.5%)	$0.854_{-0.070}^{+0.049}$ (7.0%)
γ^3	-	(0, 2.0)	-	$0.958_{-0.635}^{+0.728}$ (71.2%)	$0.795_{-0.046}^{+0.057}$ (6.5%)
b_v^1	-	(-10, 10)	-	$1.142_{-1.676}^{+1.071}$ (120.2%)	$1.380_{-0.352}^{+0.374}$ (26.3%)
b_v^2	-	(-10, 10)	-	$1.932_{-3.504}^{+2.136}$ (145.9%)	$3.185_{-0.701}^{+0.869}$ (24.6%)
b_v^3	-	(-10, 10)	-	$2.595_{-4.406}^{+3.282}$ (148.1%)	$5.724_{-1.534}^{+1.857}$ (29.6%)

where $P_{\text{data}}^{\text{AB}}(k, z)$ and $P_{\text{th}}^{\text{AB}}(k, z)$ are the mock data and the theoretical power spectrum at z , respectively, and σ_{data} is the error of the mock data. Then the likelihood function can be estimated by $\mathcal{L} \propto \exp(-\chi^2/2)$. The total chi-square for joint constraint can be estimated by $\chi_{\text{joint}}^2 = \chi_{\text{gg}}^2 + \chi_{\text{vv}}^2 + \chi_{\text{vg}}^2$, where $\chi_{\text{gg}}^2, \chi_{\text{vv}}^2$ and χ_{vg}^2 are the chi-squares for the galaxy, void and void-galaxy power spectra.

We constrain the free parameters in our fitting process using the MCMC method by `emcee` (Foreman-Mackey et al. 2013; Goodman & Weare 2010). We choose 112 walkers and obtain 30000 steps for each walker. The first 3000 steps have been removed as the burn-in process, and after thinning the chains, we obtain 30,000 chain points for illustrating the probability distribution

functions (PDFs) of the free parameters. In Table 2, we list the fiducial values and flat priors for the cosmological and void parameters. The free cosmological parameters includes dark energy equation of state w , reduced Hubble constant h , spectral index n_s , and amplitude of initial power spectrum A_s , the total matter density parameter Ω_m , and baryon density parameter Ω_b . Note that the fiducial value of A_s is derived by $\sigma_8 = 0.8102$ from Jiutian simulation. Note that, since the free parameters about void density profile, i.e. α, β and γ , are not the input parameters in the simulation, they do not have the fiducial values.

Besides, the flat priors of the systematical parameters are $b_g^i \in (0, 3.0)$, $b_v^i \in (-10.0, 10.0)$, $\log_{10}(N_g^i) \in (3.0, 5.0)$, $\log_{10}(N_v^i) \in (0, 10.0)$ and $\log_{10}(N_{\text{vg}}^i) \in$

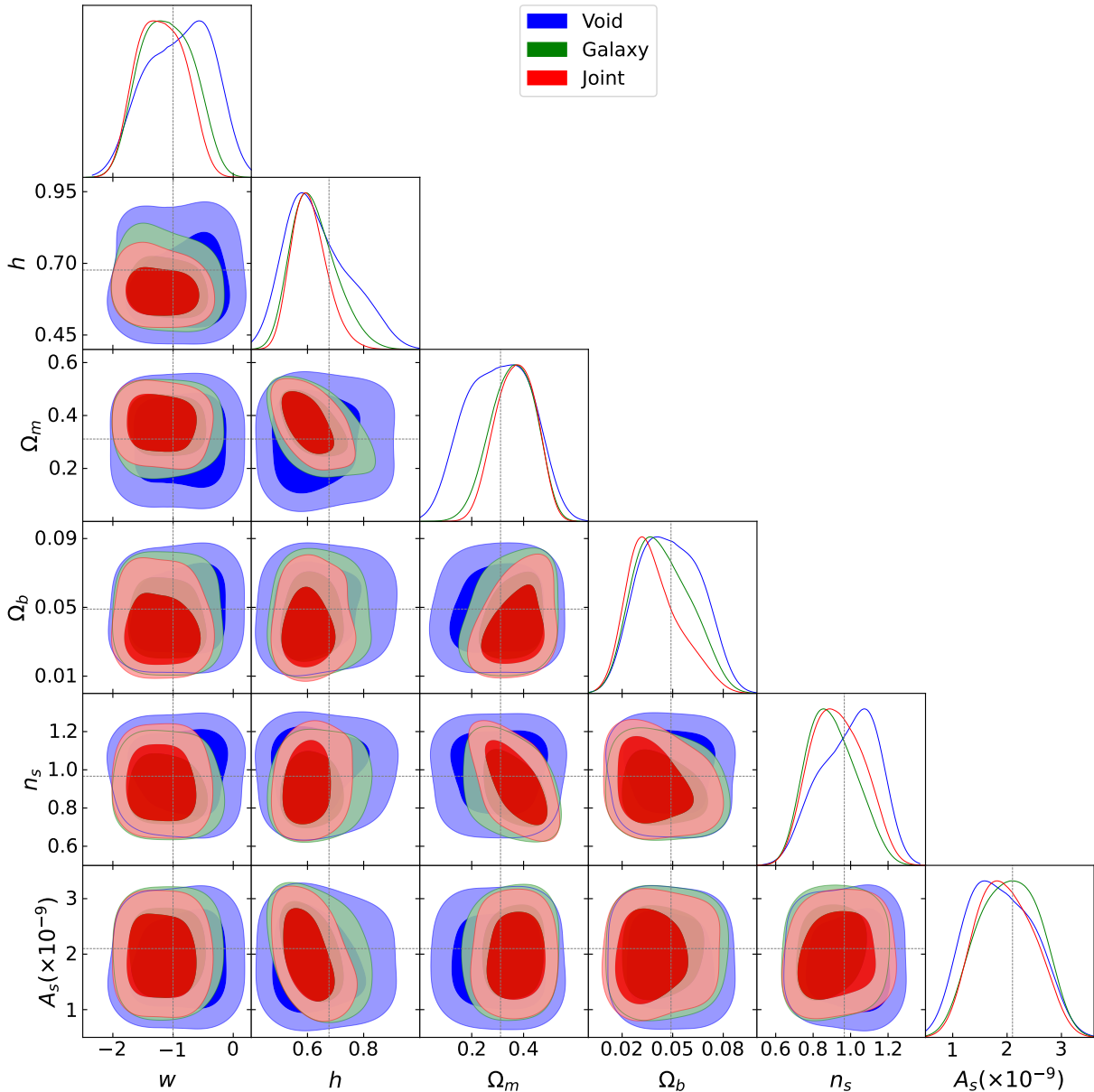


Figure 2. Contour maps of the six cosmological parameters at 68% and 95% CL for galaxy clustering (green), void clustering (blue) and joint constraints (red) derived from the simulation. The 1D PDF for each parameter is also shown. The gray dotted lines mark the fiducial values of the cosmological parameters.

$(-10.0, 10.0)$ at a given redshift. In the joint constraint, to obtain better constraint results, we consider the fitting results from the galaxy auto power spectra, and set tighter prior ranges for N_g^i with the lower bounds 1×10^3 , 2×10^3 and $3 \times 10^3 (\text{Mpc}/h)^{-3}$ at the three redshifts. In our fitting process, we totally have 30 free parameters, which contain 6 cosmological parameters, 3 void parameters at each redshift, and 15 systematical parameters.

In Figure 2, we show the constraint results of the cosmological parameters from galaxy clustering only, void power spectrum only, and joint constraint. The best-

fit values, 1σ errors and relative accuracies for the cosmological parameters are listed in Table 2. Note that the current constraint accuracies are derived from the simulations limited by the box size, and it will be improved by about one order of magnitude for the real CSST full sky survey with $17,500 \text{ deg}^2$. The best-fit curves of the void, galaxy and void-galaxy power spectra, and the clustering and noise terms are shown in Figure 1.

We can find that the best-fit curves can match the data points of the power spectra very well (see Figure 1), and the fitting results of the cosmological parameters are

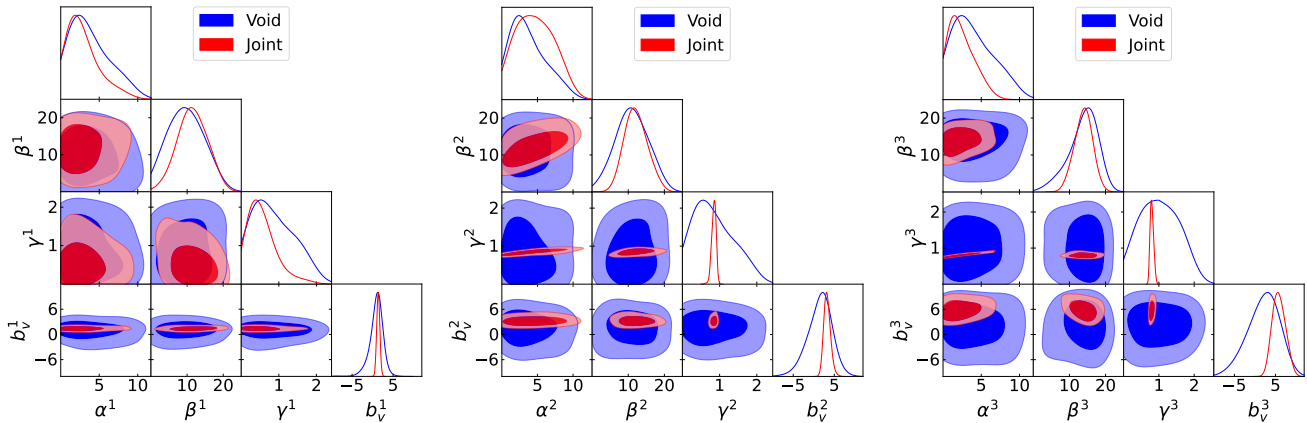


Figure 3. Contour maps at 68% and 95% CL and 1D PDFs of the three void density profile parameters and void biases constrained by the void auto power spectra (blue) and joint power spectra (red) derived from the simulation. The left, middle and right panels show the results of α^i , β^i , γ^i and b_v^i at $z = 0.3, 0.6$ and 0.9 , respectively.

consistent with the fiducial values within or close to 1σ confidence level (CL) (see Figure 2). This means that our theoretical model can explain the data and extract the cosmological information correctly, especially for the modeling of the void auto power spectrum and void-galaxy cross power spectrum.

We also notice that, as shown in Figure 1, the void power spectrum is actually dominated by the noise term, particularly at high redshifts, due to large shot noise or low number density, which may limit its constraint accuracy on the cosmological parameters. However, after considering the void-galaxy power spectrum, the joint fitting can improve the constraint accuracies by as large as $\sim 20\%$ compared to that from the galaxy power spectrum only. This indicates that the probe of void and void-galaxy power spectra can be complementary to the galaxy clustering measurement for extracting cosmological information, especially for the next generation of surveys, e.g. CSST, covering large sky areas with high magnitude limits.

In Figure 3, we show the contour maps and 1D PDFs of α , β , γ and b_v derived from the void power spectrum only and joint constraint. We can find that the best-fit values of α are similar at the three redshifts, which give $\alpha \sim 3$. For β and γ , it has some trend that both of them become larger at higher redshifts, which varies from 10 to 15 for β and from 0.4 to 0.9 for γ , although the best-fit values are consistent within 1σ at the three redshifts. This is also consistent with expectations, that the density profile of voids becomes flatter and shallower at high redshifts. Besides, the joint constraints can effectively improve the constraint accuracies of the void parameters, especially for γ , which is because the cosmological and systematical parameters can be better constrained

in this case. These results can provide reference and be significantly improved in future galaxy surveys.

For the constraint on b_v , we note that the joint power spectra can effectively improve the constraint accuracy by several times or even one order of magnitude, compared to the case using the void auto power spectra only (see also Table 2). We can also find that the probability distributions of b_v at the three redshifts cover both positive and negative values while the positions of the peaks are positive, if only considering the void auto power spectrum. On the other hand, the probability distributions of b_v are mainly in the positive regions if using the joint power spectra. This is because that, since the void bias is usually negative at large scales and positive at small scales (see e.g. Hamaus et al. 2014b; Chan et al. 2014), and our mock data at small scales with much smaller errors are dominant (see Figure 1), especially for the void-galaxy power spectra, the current results are reasonable and expectable.

Besides the void bias b_v , the other systematical parameters in the theoretical models of the galaxy power spectrum, void power spectrum and void-galaxy power spectrum are also jointly constrained, such as the galaxy bias b_g , and noise terms N_g , N_v and N_{vg} at different redshifts. The constraint results of these parameters are shown in the Appendix, and we can find that these parameters are also well constrained in our analysis.

5. SUMMARY AND CONCLUSION

In this work, we study the constraints on the cosmological and void parameters using the void and galaxy clustering mock data measured by the CSST spectroscopic survey. The Jiutian simulation is used to obtain the galaxy mock catalog at $z = 0.3, 0.6$, and 0.9 , considering the CSST instrumental design and survey strategy. We identify voids from the galaxy catalogs by VIDE

which adopts the watershed algorithm, and generate the void mock catalogs. Then the void power spectrum, galaxy power spectrum, and void-galaxy cross power spectrum at each redshift are derived. In order to fit the data, we propose to use the mean void effective radius R_v^{mean} at a given redshift to simplify the theoretical model. The MCMC method are employed to perform the constraint, and the systematical parameters are also considered in the fitting process.

We find that our theoretical model can fit the galaxy, void and void-galaxy power spectra very well, and the best-fits of the cosmological parameters are consistent with their fiducial values within or close to 1σ CL, which demonstrates the feasibility of our modeling. Besides, the joint constraints including all galaxy and void power spectra can effectively improve the constraint accuracy of the cosmological parameters by $\sim 20\%$, compared to the result derived from the galaxy power spectrum only. This indicates that the void clustering measurement can be a good complement to the galaxy clustering probe, especially for the future wide-field galaxy surveys with large survey volumes and massive samples. For the parameters of the void density profile, i.e. α , β and γ , we also obtain stringent constraint results in the joint fitting case, and find that the void density profile becomes flatter and shallower at high redshifts, which is as expected for the properties of high- z voids.

Considering the full CSST survey area, the measurements of the void and galaxy clustering can provide constraints on the order of a few percent or even higher accuracy for the cosmological and void parameters. This means that cosmic void observations have great potential in the next-generation galaxy surveys, and can take an important role in the future cosmological studies.

YS, QX and YG acknowledge the support from National Key R&D Program of China grant Nos. 2022YFF0503404, 2020SKA0110402, and the CAS Project for Young Scientists in Basic Research (No. YSBR-092). KCC acknowledges the support the National Science Foundation of China under the grant number 12273121. XLC acknowledges the support of the National Natural Science Foundation of China through Grant Nos. 11473044 and 11973047, and the Chinese Academy of Science grants ZDKYYQ20200008, QYZDJ-SSW-SLH017, XDB 23040100, and XDA15020200. QG acknowledges the support from the National Natural Science Foundation of China (NSFC No.12033008). GLL, YL and CLW acknowledges the support from NSFC grant No. U1931210. This work is also supported by science research grants from the China Manned Space Project with Grant Nos. CMS- CSST-2021-B01 and CMS- CSST-2021-A01.

APPENDIX

We show the constraint results of the galaxy bias in Figure 4. We obtain $b_g^1 = 1.251_{-0.262}^{+0.302}$, $b_g^2 = 1.575_{-0.315}^{+0.331}$, $b_g^3 = 2.274_{-0.437}^{+0.494}$ in the joint fitting process. We can find the galaxy biases can be stringently constrained by the galaxy power spectra, and the joint constraint can provide a $\sim 15\%$ improvement on b_g^i . This indicates that it is effective to include the void-galaxy cross power spectrum for studying the galaxy bias.

In Figure 5, we show the constraint results of the noise terms in the galaxy, void and void-galaxy theoretical power spectra. We have $\log_{10}(N_g^1) =$

$3.254_{-0.176}^{+0.204}$, $\log_{10}(N_g^2) = 3.476_{-0.125}^{+0.152}$, $\log_{10}(N_g^3) = 3.699_{-0.144}^{+0.144}$, $\log_{10}(N_v^1) = 4.443_{-0.042}^{+0.059}$, $\log_{10}(N_v^2) = 5.088_{-0.026}^{+0.022}$, $\log_{10}(N_v^3) = 5.640_{-0.039}^{+0.034}$, $\log_{10}(N_{vg}^1) = 2.993_{-1.680}^{+0.569}$, $\log_{10}(N_{vg}^2) = 1.069_{-4.213}^{+1.893}$ and $\log_{10}(N_{vg}^3) = -1.369_{-4.861}^{+3.386}$ at the three redshifts in the joint fitting process. The joint constraints can provide a $\sim 50\%$ improvement on N_g at $z = 0.6$ and 0.9 and $\sim 25\%$ improvement on N_v at $z = 0.3, 0.6$ and 0.9 . We can find that the noise terms in the galaxy and void auto power spectrum increase with redshift, and N_{vg} in the void-galaxy cross power spectrum is relatively low and close to zero at high redshifts.

REFERENCES

- Achitouv, I. 2016, PhRvD, 94, 103524,
doi: [10.1103/PhysRevD.94.103524](https://doi.org/10.1103/PhysRevD.94.103524)
- Alam, S., Ata, M., Bailey, S., et al. 2017, MNRAS, 470, 2617, doi: [10.1093/mnras/stx721](https://doi.org/10.1093/mnras/stx721)
- Alcock, C., & Paczynski, B. 1979, Nature, 281, 358,
doi: [10.1038/281358a0](https://doi.org/10.1038/281358a0)
- Bond, J. R., Kofman, L., & Pogosyan, D. 1996, Nature, 380, 603, doi: [10.1038/380603a0](https://doi.org/10.1038/380603a0)

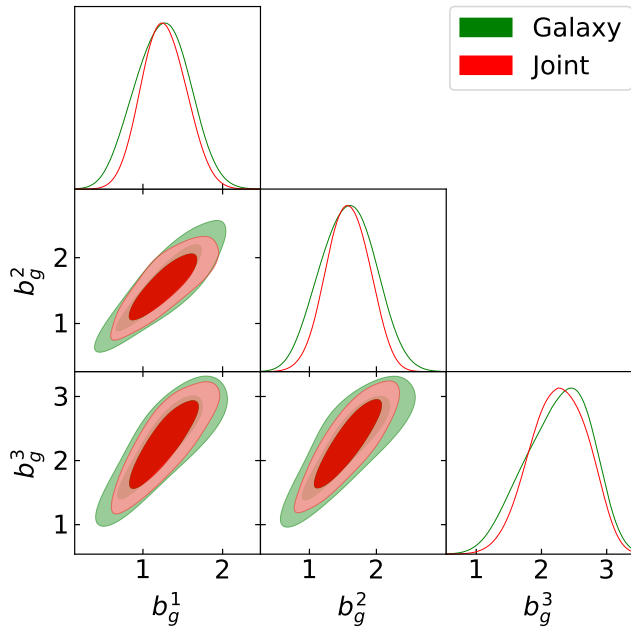


Figure 4. Contour maps at 68% and 95% CL and 1D PDFs of the galaxy bias b_g^i at $z = 0.3, 0.6$ and 0.9 derived from the galaxy power spectrum (green) and joint power spectra (red) in the simulation, respectively.

Cai, Y.-C., Padilla, N., & Li, B. 2015, MNRAS, 451, 1036, doi: [10.1093/mnras/stv777](https://doi.org/10.1093/mnras/stv777)

Cai, Y.-C., Taylor, A., Peacock, J. A., & Padilla, N. 2016, MNRAS, 462, 2465, doi: [10.1093/mnras/stw1809](https://doi.org/10.1093/mnras/stw1809)

Cao, Y., Gong, Y., Meng, X.-M., et al. 2018, MNRAS, 480, 2178, doi: [10.1093/mnras/sty1980](https://doi.org/10.1093/mnras/sty1980)

Chan, K. C., & Hamaus, N. 2021, PhRvD, 103, 043502, doi: [10.1103/PhysRevD.103.043502](https://doi.org/10.1103/PhysRevD.103.043502)

Chan, K. C., Hamaus, N., & Desjacques, V. 2014, PhRvD, 90, 103521, doi: [10.1103/PhysRevD.90.103521](https://doi.org/10.1103/PhysRevD.90.103521)

Contarini, S., Marulli, F., Moscardini, L., et al. 2021, MNRAS, 504, 5021, doi: [10.1093/mnras/stab1112](https://doi.org/10.1093/mnras/stab1112)

Contarini, S., Pisani, A., Hamaus, N., et al. 2023, ApJ, 953, 46, doi: [10.3847/1538-4357/acde54](https://doi.org/10.3847/1538-4357/acde54)

Contarini, S., Verza, G., Pisani, A., et al. 2022, A&A, 667, A162, doi: [10.1051/0004-6361/202244095](https://doi.org/10.1051/0004-6361/202244095)

Correa, C. M., Paz, D. J., Padilla, N. D., et al. 2022, MNRAS, 509, 1871, doi: [10.1093/mnras/stab3070](https://doi.org/10.1093/mnras/stab3070)

Correa, C. M., Paz, D. J., Sánchez, A. G., et al. 2021, MNRAS, 500, 911, doi: [10.1093/mnras/staa3252](https://doi.org/10.1093/mnras/staa3252)

Croton, D. J., Springel, V., White, S. D. M., et al. 2006, MNRAS, 365, 11, doi: [10.1111/j.1365-2966.2005.09675.x](https://doi.org/10.1111/j.1365-2966.2005.09675.x)

de Lapparent, V., Geller, M. J., & Huchra, J. P. 1986, ApJL, 302, L1, doi: [10.1086/184625](https://doi.org/10.1086/184625)

De Lucia, G., & Blaizot, J. 2007, MNRAS, 375, 2, doi: [10.1111/j.1365-2966.2006.11287.x](https://doi.org/10.1111/j.1365-2966.2006.11287.x)

Deng, F., Gong, Y., Wang, Y., et al. 2022, MNRAS, 515, 5894, doi: [10.1093/mnras/stac2185](https://doi.org/10.1093/mnras/stac2185)

DESI Collaboration, Aghamousa, A., Aguilar, J., et al. 2016, arXiv e-prints, arXiv:1611.00036, doi: [10.48550/arXiv.1611.00036](https://doi.org/10.48550/arXiv.1611.00036)

Falck, B., Koyama, K., Zhao, G.-B., & Cautun, M. 2018, MNRAS, 475, 3262, doi: [10.1093/mnras/stx3288](https://doi.org/10.1093/mnras/stx3288)

Foreman-Mackey, D., Hogg, D. W., Lang, D., & Goodman, J. 2013, PASP, 125, 306, doi: [10.1086/670067](https://doi.org/10.1086/670067)

Forero-Sánchez, D., Zhao, C., Tao, C., et al. 2022, MNRAS, 513, 5407, doi: [10.1093/mnras/stac1268](https://doi.org/10.1093/mnras/stac1268)

Gong, Y., Liu, X., Cao, Y., et al. 2019, ApJ, 883, 203, doi: [10.3847/1538-4357/ab391e](https://doi.org/10.3847/1538-4357/ab391e)

Goodman, J., & Weare, J. 2010, Communications in Applied Mathematics and Computational Science, 5, 65, doi: [10.2140/camcos.2010.5.65](https://doi.org/10.2140/camcos.2010.5.65)

Gregory, S. A., & Thompson, L. A. 1978, ApJ, 222, 784, doi: [10.1086/156198](https://doi.org/10.1086/156198)

Guo, Q., White, S., Boylan-Kolchin, M., et al. 2011, MNRAS, 413, 101, doi: [10.1111/j.1365-2966.2010.18114.x](https://doi.org/10.1111/j.1365-2966.2010.18114.x)

Hamaus, N., Sutter, P. M., & Wandelt, B. D. 2014a, PhRvL, 112, 251302, doi: [10.1103/PhysRevLett.112.251302](https://doi.org/10.1103/PhysRevLett.112.251302)

Hamaus, N., Wandelt, B. D., Sutter, P. M., Lavaux, G., & Warren, M. S. 2014b, PhRvL, 112, 041304, doi: [10.1103/PhysRevLett.112.041304](https://doi.org/10.1103/PhysRevLett.112.041304)

Hamaus, N., Aubert, M., Pisani, A., et al. 2022, A&A, 658, A20, doi: [10.1051/0004-6361/202142073](https://doi.org/10.1051/0004-6361/202142073)

Henriques, B. M. B., White, S. D. M., Thomas, P. A., et al. 2015, MNRAS, 451, 2663, doi: [10.1093/mnras/stv705](https://doi.org/10.1093/mnras/stv705)

Jõeveer, M., Einasto, J., & Tago, E. 1978, MNRAS, 185, 357, doi: [10.1093/mnras/185.2.357](https://doi.org/10.1093/mnras/185.2.357)

Khoraminezhad, H., Vielzeuf, P., Lazeyras, T., Baccigalupi, C., & Viel, M. 2022, MNRAS, 511, 4333, doi: [10.1093/mnras/stac331](https://doi.org/10.1093/mnras/stac331)

Kirshner, R. P., Oemler, A., J., Schechter, P. L., & Shectman, S. A. 1981, ApJL, 248, L57, doi: [10.1086/183623](https://doi.org/10.1086/183623)

Kreisch, C. D., Pisani, A., Carbone, C., et al. 2019, MNRAS, 488, 4413, doi: [10.1093/mnras/stz1944](https://doi.org/10.1093/mnras/stz1944)

Kreisch, C. D., Pisani, A., Villaescusa-Navarro, F., et al. 2022, ApJ, 935, 100, doi: [10.3847/1538-4357/ac7d4b](https://doi.org/10.3847/1538-4357/ac7d4b)

Lewis, A., Challinor, A., & Lasenby, A. 2000, ApJ, 538, 473, doi: [10.1086/309179](https://doi.org/10.1086/309179)

Mauland, R., Elgarøy, Ø., Mota, D. F., & Winther, H. A. 2023, A&A, 674, A185, doi: [10.1051/0004-6361/202346287](https://doi.org/10.1051/0004-6361/202346287)

Miao, H., Gong, Y., Chen, X., et al. 2023, MNRAS, 519, 1132, doi: [10.1093/mnras/stac3583](https://doi.org/10.1093/mnras/stac3583)

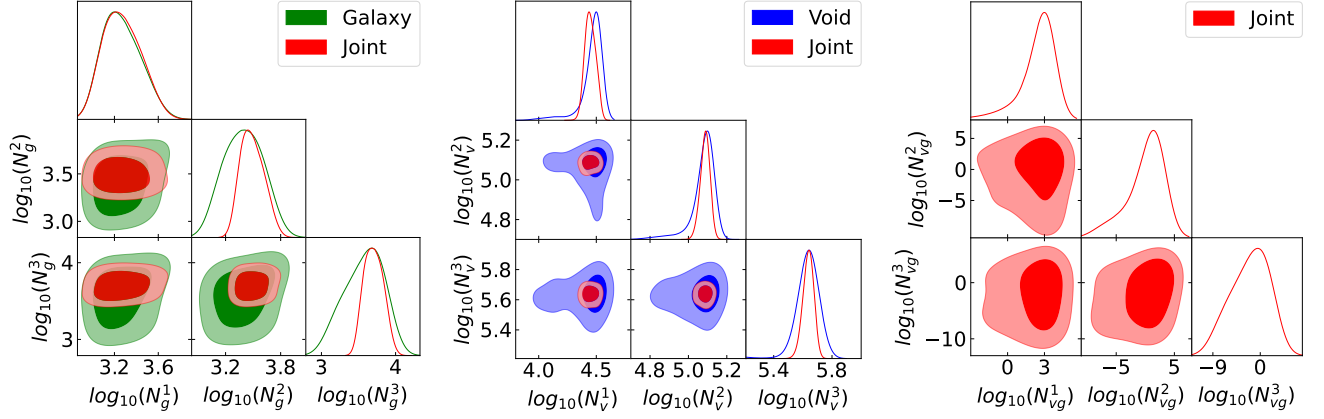


Figure 5. Contour maps at 68% and 95% CL and 1D PDFs of N_g^i (left panel), N_v^i (middle panel) and N_{vg}^i (right panel) at $z = 0.3, 0.6$ and 0.9 derived from the galaxy power spectrum (green), void power spectrum (blue) and joint power spectra (red) in the simulation, respectively.

Murray, S. G. 2018, *The Journal of Open Source Software*, 3, 850, doi: [10.21105/joss.00850](https://doi.org/10.21105/joss.00850)

Nadathur, S., & Percival, W. J. 2019, *MNRAS*, 483, 3472, doi: [10.1093/mnras/sty3372](https://doi.org/10.1093/mnras/sty3372)

Nadathur, S., Woodfinden, A., Percival, W. J., et al. 2020, *MNRAS*, 499, 4140, doi: [10.1093/mnras/staa3074](https://doi.org/10.1093/mnras/staa3074)

Neyrinck, M. C. 2008, *MNRAS*, 386, 2101, doi: [10.1111/j.1365-2966.2008.13180.x](https://doi.org/10.1111/j.1365-2966.2008.13180.x)

Paillas, E., Cautun, M., Li, B., et al. 2019, *MNRAS*, 484, 1149, doi: [10.1093/mnras/stz022](https://doi.org/10.1093/mnras/stz022)

Pei, W., Guo, Q., Li, M., et al. 2024, *MNRAS*, 529, 4958, doi: [10.1093/mnras/stae866](https://doi.org/10.1093/mnras/stae866)

Pellicciari, D., Contarini, S., Marulli, F., et al. 2023, *MNRAS*, 522, 152, doi: [10.1093/mnras/stad956](https://doi.org/10.1093/mnras/stad956)

Perico, E. L. D., Voivodic, R., Lima, M., & Mota, D. F. 2019, *A&A*, 632, A52, doi: [10.1051/0004-6361/201935949](https://doi.org/10.1051/0004-6361/201935949)

Pisani, A., Sutter, P. M., Hamaus, N., et al. 2015, *PhRvD*, 92, 083531, doi: [10.1103/PhysRevD.92.083531](https://doi.org/10.1103/PhysRevD.92.083531)

Planck Collaboration, Aghanim, N., Akrami, Y., et al. 2020, *A&A*, 641, A6, doi: [10.1051/0004-6361/201833910](https://doi.org/10.1051/0004-6361/201833910)

Platen, E., van de Weygaert, R., & Jones, B. J. T. 2007, *MNRAS*, 380, 551, doi: [10.1111/j.1365-2966.2007.12125.x](https://doi.org/10.1111/j.1365-2966.2007.12125.x)

Pollina, G., Baldi, M., Marulli, F., & Moscardini, L. 2016, *MNRAS*, 455, 3075, doi: [10.1093/mnras/stv2503](https://doi.org/10.1093/mnras/stv2503)

Radinović, S., Nadathur, S., Winther, H. A., et al. 2023, *A&A*, 677, A78, doi: [10.1051/0004-6361/202346121](https://doi.org/10.1051/0004-6361/202346121)

Sahlén, M., & Silk, J. 2018, *PhRvD*, 97, 103504, doi: [10.1103/PhysRevD.97.103504](https://doi.org/10.1103/PhysRevD.97.103504)

Sahlén, M., Zubeldía, Í., & Silk, J. 2016, *ApJL*, 820, L7, doi: [10.3847/2041-8205/820/1/L7](https://doi.org/10.3847/2041-8205/820/1/L7)

Schuster, N., Hamaus, N., Pisani, A., et al. 2019, *JCAP*, 2019, 055, doi: [10.1088/1475-7516/2019/12/055](https://doi.org/10.1088/1475-7516/2019/12/055)

Scoccimarro, R. 2004, *PhRvD*, 70, 083007, doi: [10.1103/PhysRevD.70.083007](https://doi.org/10.1103/PhysRevD.70.083007)

Song, Y., Xiong, Q., Gong, Y., et al. 2024, *MNRAS*, 532, 1049, doi: [10.1093/mnras/stae1575](https://doi.org/10.1093/mnras/stae1575)

Springel, V. 2005, *MNRAS*, 364, 1105, doi: [10.1111/j.1365-2966.2005.09655.x](https://doi.org/10.1111/j.1365-2966.2005.09655.x)

Springel, V., Yoshida, N., & White, S. D. M. 2001, *NewA*, 6, 79, doi: [10.1016/S1384-1076\(01\)00042-2](https://doi.org/10.1016/S1384-1076(01)00042-2)

Sutter, P. M., Lavaux, G., Hamaus, N., et al. 2015, *Astronomy and Computing*, 9, 1, doi: [10.1016/j.ascom.2014.10.002](https://doi.org/10.1016/j.ascom.2014.10.002)

Taruya, A., Nishimichi, T., & Saito, S. 2010, *PhRvD*, 82, 063522, doi: [10.1103/PhysRevD.82.063522](https://doi.org/10.1103/PhysRevD.82.063522)

Verza, G., Carbone, C., Pisani, A., Porciani, C., & Matarrese, S. 2024, arXiv e-prints, arXiv:2401.14451, doi: [10.48550/arXiv.2401.14451](https://doi.org/10.48550/arXiv.2401.14451)

Verza, G., Carbone, C., Pisani, A., & Renzi, A. 2023, *JCAP*, 2023, 044, doi: [10.1088/1475-7516/2023/12/044](https://doi.org/10.1088/1475-7516/2023/12/044)

Verza, G., Pisani, A., Carbone, C., Hamaus, N., & Guzzo, L. 2019, *JCAP*, 2019, 040, doi: [10.1088/1475-7516/2019/12/040](https://doi.org/10.1088/1475-7516/2019/12/040)

Vielzeuf, P., Calabrese, M., Carbone, C., Fabbian, G., & Baccigalupi, C. 2023, *JCAP*, 2023, 010, doi: [10.1088/1475-7516/2023/08/010](https://doi.org/10.1088/1475-7516/2023/08/010)

Wang, X., Chen, X., Zheng, Z., et al. 2009, *MNRAS*, 394, 1775, doi: [10.1111/j.1365-2966.2009.14468.x](https://doi.org/10.1111/j.1365-2966.2009.14468.x)

Woodfinden, A., Nadathur, S., Percival, W. J., et al. 2022, *MNRAS*, 516, 4307, doi: [10.1093/mnras/stac2475](https://doi.org/10.1093/mnras/stac2475)

Zhan, H. 2011, *Scientia Sinica Physica, Mechanica & Astronomica*, 41, 1441, doi: [10.1360/132011-961](https://doi.org/10.1360/132011-961)

Zhan, H. 2021, *Chinese Science Bulletin*, 66, 1290, doi: [10.1360/TB-2021-0016](https://doi.org/10.1360/TB-2021-0016)

Zivick, P., Sutter, P. M., Wandelt, B. D., Li, B., & Lam, T. Y. 2015, *MNRAS*, 451, 4215, doi: [10.1093/mnras/stv1209](https://doi.org/10.1093/mnras/stv1209)